Journal Pre-proof

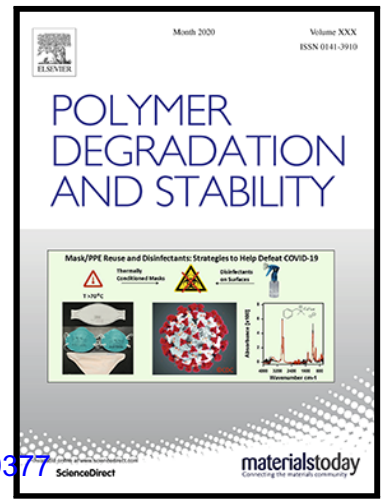

Effect of Silica Aerogel – Aluminium Trihydroxide Hybrid Filler on the Physio-mechanical and Thermal Decomposition Behaviour of Unsaturated Polyester Resin Composite

Zulhelmi Alif Abdul Halim , Muhamad Azizi Mat Yajid , Fajar Anugrah Nurhadi , Norhayati Ahmad , Halimaton Hamdan

PII: S0141-3910(20)30307-4
DOI: https://doi.org/10.1016/j.polymdegradstab.2020.109377
Reference: PDST 109377

To appear in: *Polymer Degradation and Stability*

Received date: 7 July 2020
Revised date: 12 September 2020
Accepted date: 26 September 2020

Please cite this article as: Zulhelmi Alif Abdul Halim , Muhamad Azizi Mat Yajid , Fajar Anugrah Nurhadi , Norhayati Ahmad , Halimaton Hamdan , Effect of Silica Aerogel – Aluminium Trihydroxide Hybrid Filler on the Physio-mechanical and Thermal Decomposition Behaviour of Unsaturated Polyester Resin Composite, *Polymer Degradation and Stability* (2020), doi: https://doi.org/10.1016/j.polymdegradstab.2020.109377

Highlights

- **Aluminum trihydroxide and silica aerogel as hybrid filler for unsaturated polyester**
- **The hybrid filler provides advantages concerning thermal stability and density**
- **The hybrid filler exert a synergistic thermal effect on polyester composite**
- **The hybrid filler contributes small increase in tensile strength in the present form**

Effect of Silica Aerogel – Aluminium Trihydroxide Hybrid Filler on the Physio-mechanical and Thermal Decomposition Behaviour of Unsaturated Polyester Resin Composite

Zulhelmi Alif Abdul Halim[1, a*], Muhamad Azizi Mat Yajid[1,b], Fajar Anugrah Nurhadi[1,c], Norhayati Ahmad[1,d] and Halimaton Hamdan[2,e]

[1]School of Mechanical Engineering, Universiti Teknologi Malaysia, 81310, Johor, Malaysia

[2]Zeolite and Nanostructured Materials Laboratory, Universiti Teknologi Malaysia, 81310, Johor, Malaysia

[a]zulhelmialif@utm.my ([*]corresponding author), [b]azizi_my@fkm.utm.my, [c]fajaranugrahnurhadi@gmail.com, [d]nhayatiahmad@utm.my, [e]hali@kimia.fs.utm.my

Abstract

Aluminum trihydroxide (ATH) is an eco-friendly and economical additive used in polymers as a flame retardant (FR), but its low thermal stability has become an important issue that is critical in determining the fire protection and thermal stability of the composites. The present study was an attempt to enhance the thermal stability of ATH to some extent by combining it with nano-porous silica known as silica aerogel (SA) as a hybrid FR filler in unsaturated polyester resin (UPR). Ultra-low density SA (0.07 g/cm^3) in the form of fine particles was extracted from renewable resources (i.e. rice husk), through a sol-gel process, surface modification and dried at atmospheric pressure. From our findings, it is found that the addition of the hybrid filler into UPR results in interesting properties such as lightweight, flame retardancy and enhanced thermal stability whose properties cannot be gained by composites with single filler. From thermogravimetric analysis (TGA), differential scanning calorimetry (DSC) and gas analysis using Fourier transform infrared spectroscopy (FTIR); it is evident that doping the ATH with SA helps to improve the thermal stability via synergistic effect, by extending the ATH decomposition process over a wider temperature range. As a result, the UPR filled with SA/ATH hybrid demonstrates higher thermal stability when compared to the composites filled with only ATH or SA. Furthermore, the SA/ATH hybrid also provides sufficient flame retardancy in UPR as evaluate by ASTM D635-14 (UL–94) horizontal burning test. For mechanical properties, a sharp increase in tensile strength was observed for UPR filled with ATH or SA while the addition of SA/ATH hybrid filler only slightly increases the tensile properties of UPR due to particle agglomerations and porosities.

Keywords: Silica aerogel; Aluminium trihydroxide; Unsaturated polyester resin; Synergism; Polymer composites; Filler

Acknowledgment

The author would like to thank the Research Management Centre (RMC) of Universiti Teknologi Malaysia for funding this project through Post-Doctoral Fellowship Scheme for the project: Design and Development of Eco-Friendly Silica-Alumina Hybrid Flame Retardant for Commodity Plastics.

1.0 Introduction

Dramatic increases in the use of highly flammable polymers and strict safety standards have created a large market for flame retardant (FR) additives [1]. Unsaturated polyester resin (UPR) is the most commercially important thermosetting resins and its flame retardancy has attracted great attention [2–5]. Recently, the use of low smoke, free of halogen (LSFOH) mineral hydrates as FR additives in UPR has been trending due to growing consumer awareness of toxicity issues and support from governments for "green" products [6-7]. Aluminum trihydroxide (ATH) is the active FR filler most often used in commodity polymers, particularly for UPR since it is cost-effective, environmentally friendly and easy to apply into polymers [8]. The FR mechanism of ATH involves its thermal degradation through a single step endothermic process, releasing the water vapor at temperatures of 200 °C - 300 °C and forming a thermally stable residue made of aluminum oxide (Al_2O_3) [8]. During polymer combustion, the water vapor will act as a diluting agent in the gas phase and decreasing the temperature in the system while the residue of Al_2O_3 builds up to form a protective layer [8].

It is expected that the demand for ATH will continue to outpace other FR materials in the coming years especially when sustainable flame retardant technology is coming to the forefront [6]. However, one on-going problem with the use of ATH in polymers and plastics is related to the high loading requirement of ATH for sufficient flame retardance. High ATH concentrations will result in high processing viscosity which often reduces processability but more importantly, increasing the density [9]. Another important issue is the thermal stability of ATH which is the essential factor to evaluate its effectiveness in polymers. ATH starts to decompose at relatively lower temperatures than that of some polymers, particularly thermoplastics that require high processing temperature and thermally stable thermosets [9]. In the case of UPR, the pyrolysis and combustion behavior of the polymer have been reviewed and studied extensively [10]. Although the addition of ATH at an adequate level can impart flame resistance in UPR [10], it has a little effect on the thermal stability due to its considerably low dehydration temperature which is limited between 200 °C to 300 °C. When the UPR is subjected to prolonged heating, fire can still occur via self-ignition at a high temperature of around 330 ºC [11]. For that reason, there is a significant need to improve the thermal stability of the current commercial grade of ATH to match with the characteristics of the polymers.

As previously described in the literature for UPR [10, 12-16], researchers have proposed various combinations between ATH and other materials to create a synergistic effect on flame retardancy and thermal stability of polymer through formations of thermostable active compounds, intumescent chars, and chemical interaction [15-17]. To date, ATH has been used in combination with phosphorus-based FRs, ammonium polyphosphate, zinc hydroxystannate, magnesium hydrate, nanoalumina, fumed silica, expandable graphite and nanoclays [10]. Despite their effective synergisms, very few attempts were made to combine ATH with silica aerogel (SA) as a hybrid FR in UPR. SA is a micro/mesoporous material that exhibits interesting properties such as high surface area (500 – 1000 $m^2.g^{-1}$), ultra-low density (less than 0.1 $g.cm^{-3}$), hydrophobicity, high thermal stability (~1200 °C) and remarkable thermal insulation properties (<0.1 W/mK) [18]. Thanks to its rigid 3-dimensional network structure with many nano-sized pores, the SA was found very effective as a barrier for both heat and mass transport in polymers [19-21]. When compared to other materials, SA has a clear advantage in terms of lightweight-ness that can be utilized for the development of lightweight-flame retardant polymer composites.

In this study, the use of bio-derived SA is proposed to match with the eco-friendly features of ATH. The SA was synthesized from rice husk ash by the sol-gel method and dried under atmospheric pressure. The method of SA production followed our previous works [22-23]. Considering the unique physical properties of SA, combination with ATH into SA/ATH hybrid is expects to create a synergistic effect on thermal stability. The physical confinement of ATH into porous SA can be an effective strategy to restrict heat and mass transfers which could prolong the dehydration of ATH for a wider temperature range and consequently enhance the thermal stability of the host polymer. Herein, UPR composites containing ATH, SA and the hybrid were prepared and their physio-mechanical and thermal properties were studied. Through comparative analysis, the synergism between ATH and SA on fire resistance and thermal stability of UPR were proposed.

2.0 Experimental Details

2.1 Materials

Pre-accelerated, orthophthalic unsaturated polyester resin (UPR) with a styrene content of 35% by weight (commercial name Reversol P-9509) and methyl ethyl ketone peroxide (MEKP) were supplied by Revertex Pvt. Ltd. (Malaysia). Fig. 1 (a) shows the submicron aluminum trihydroxide (ATH) ($Al_2O_3.3H_2O$) of 99.6% purity, containing 34.6% water from its total molecular weight as manufactured by Huber Engineered Materials (Malaysia). The ATH particles whose size is less than 10 μm (Fig. 1 (c)) or ranging between 0.8 μm to 2.0 μm according to the manufacturer is used as a flame retardant (FR). The preparation of hydrophobic silica aerogel (SA) as depicted in Fig. 1 (b) followed our previous works [22-23]. Silica was leached from white rice husk ash by sodium hydroxide (NaOH) solution to form a sodium silicate solution. The SA was prepared via the sol-gel process, hydrophobic modification using a silane modifier and ambient pressure drying. As shown in Fig. 1 (d), the SA exhibits a micro/mesoporous structure with pore sizes in the nano to micron range. Table 1 describes the comparison of the basic properties between ATH and SA. Meanwhile, Fig. 2 shows the SEM micrograph of combined SA and ATH particles (denoted hereafter as SA/ATH hybrid) which have particle sizes ranging from a few microns to 100 μm in diameter. The SA/ATH hybrid was prepared by physically mixing the ATH and SA at equal volume using ball mixing for 15 min and further homogenized by a compact mixer shaker (KS 15A, Edmund Buhler GmbH) at 200 rpm for 15 min.

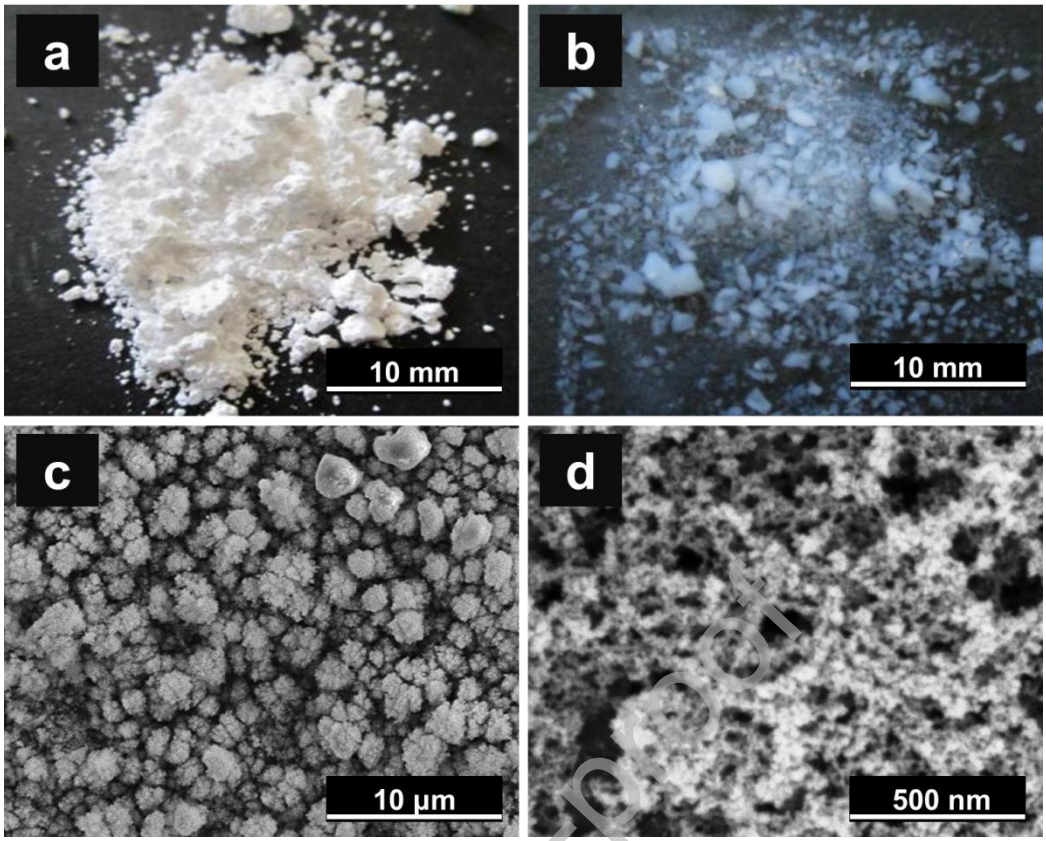

Fig. 1 Photograph and SEM micrograph of filler materials (a) Photo of ATH particles (b) Photo of SA particles (c) SEM micrograph of ATH at 2000× magnification (d) SEM micrograph of SA at 20k× magnification

Table 1: Some basic properties of ATH and SA

Property	ATH	SA
Bulk density (g/cm^3)	2.43	0.07–0.08
Particle size (µm)	0.8–2.0	50–100
Porosity (%)	Not measured	90–95
Specific surface area (m^2/g)	2–14	600–700
Surface polarity	Hydrophilic	Hydrophobic

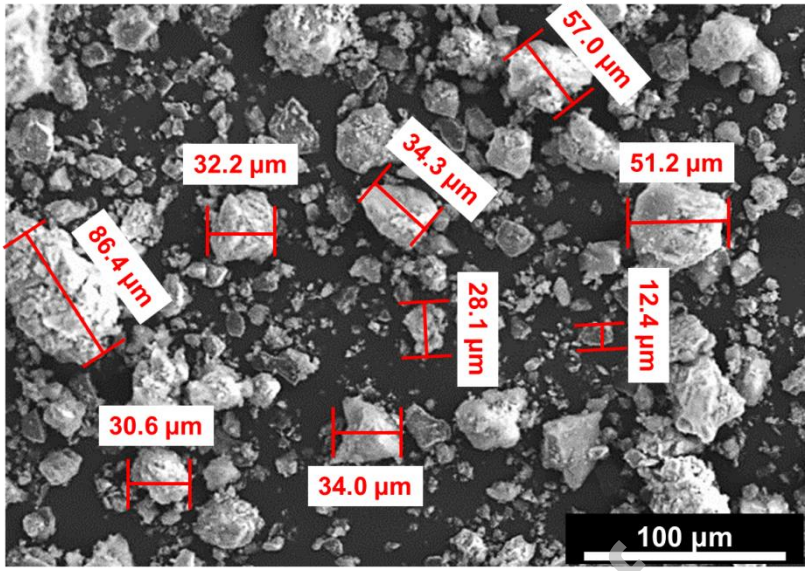

Fig. 2 Particle size distribution of SA/ATH hybrid measured by SEM

2.2 Preparation of samples

UPR composites incorporating ATH, SA and SA/ATH hybrid as fillers were prepared by the direct mixing method. Using an overhead stirrer (Daihan HS-50A, Daihan Scientific, Korea), the composites mixtures were thoroughly blended for 10 min. Then, 1% MEKP was added (based on resin volume) and the mixtures were blended again for another 10 min until the color of the mixtures changed from hazy pink to clear. The resulting mixtures were degassed under vacuum and put into an ultrasonic bath for 10 min to ensure a homogenized distribution of the particles. Then, the mixtures were poured into silicone molds to prepare specimens for the subsequent characterization and cured at room temperature for 24 h. Neat UPR specimens were also prepared for comparison. Table 2 lists the prepared compositions and the corresponding volume and weight fractions of the components. Fig. 3 illustrates the proposed molecular interaction between SA, ATH and UPR. UPR is a long linear polymer chain containing many carbon double bonds (C=O, C=C) while the styrene monomer also contains carbon double bonds that act as a curing agent by bridging adjacent polymer molecules at their unsaturation points [24]. The ATH contains a large number of hydroxyl groups and interaction with UPR is possible through the hydroxyl hydrogen (–OH) from ATH with the carbonyl oxygen (C=O) from the polar ester linkage [25]. Meanwhile, SA contains both polar and non-polar surface groups. The surface silanol groups (Si–OH) can form hydrogen bonds with the ester linkage and also with the hydroxyl from ATH (hybrid) while the methyl silyl groups (Si–CH3) are attached to other non-polar portion of the UPR (e.g. styrene crosslinks) via carbon-carbon bonds.

Table 2: Composition of composite samples prepared in this study

Sample label	UPR (ρ = 1.15 g/cm^3)		ATH (ρ = 2.43 g/cm^3)		SA (ρ = 0.08 g/cm^3)	
	vol%	wt%	vol%	wt%	vol%	wt%
UPR	100	100	0	0	0	0
UPR/30ATH	70	52.48	30	47.52	0	0
UPR/15ATH15SA	70	68.05	15	30.93	15	1.02
UPR/30SA	70	97.1	0	0	30	2.9

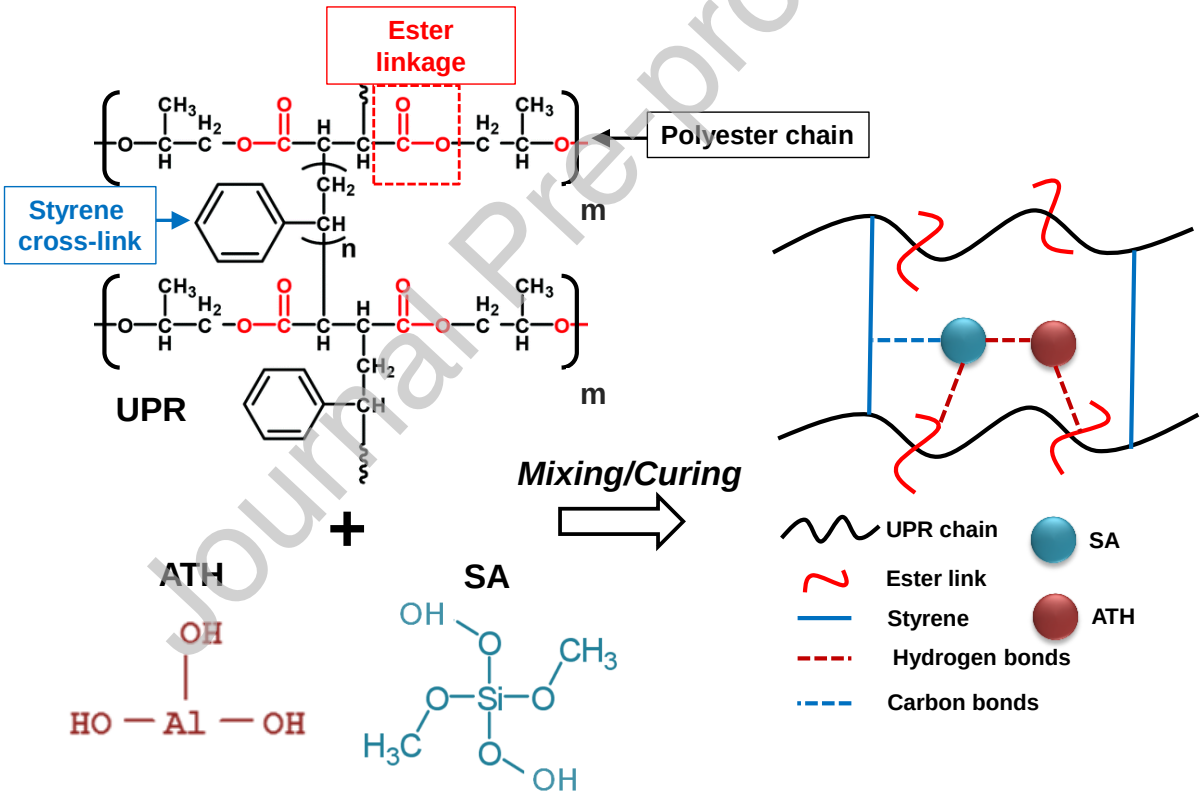

Fig. 3 Schematic representation of the interaction between filler surface with polymer chain

2.3 Characterizations

The experimental density (bulk) of the composite samples was determined by the Archimedes principle as per ASTM D792-13 with a Shimadzu AY220 analytical balance (Shimadzu Corp, Japan). At least five specimens were measured for each sample. The theoretical density of the composite samples was calculated through the volume rule of mixture, as the density of UPR, ATH and SA were known. From a comparison between the experimental and theoretical density, the volume fraction of pores or relative porosity (ϕ) could then be calculated. The tensile properties were determined using a universal testing machine (Instron 4467, Instron Corp., Canton (MA), USA) at a crosshead speed of 1.0 mm min^{-1} until failure. The test was performed on dumbbell-shaped specimens with 3.0 mm thickness (ASTM D638 Type IV) prepared by casting. Three specimens were tested for each sample and the data were averaged. Subsequently, the fracture surface obtained after the tensile test was examined under scanning electron microscopy (SEM-SU3500, Hitachi High-Technologies Co., Ltd. Japan) and the morphology and filler distribution were analyzed using energy dispersive X-ray (EDX, Oxford Instrument, UK). The flammability of the composites was evaluated according to ASTM D635-14 (Horizontal burning rate determination) which is equivalent to UL-94 for horizontal burning. The specimens were fabricated to dimensions of 100 × 12 × 3 mm. TGA measurement was performed using TGA 2 (Mettler Toledo, USA) on specimens of approximately 10–15 mg at a heating rate of 10 °C/min, up to 600 ºC under air atmospheres. Fourier transform infrared spectroscopy (FTIR, Nicolet iS10, Thermo Fisher Scientific, USA) is coupled to the TGA to measure the concentration of the different combustion gas species in the absorption frequency range of 4500–400 cm^{-1}. DSC analysis was carried out using DSC214-Polyma (NETZSCH-Gerätebau GmbH, Germany) in a closed aluminum crucible with a pierced hole in the cover. All specimens with a mass of approximately 10 mg each were heated (heating scans) from room to 400 °C at 10 °C/min under the air atmosphere.

3.0 Results and discussions

3.1 Densities and porosities of composites

Table 3 reports the theoretical and experimental (bulk) densities of the composites along with the corresponding porosities. The neat UPR and UPR/30ATH have a measured density of 1.14 g/cm^3 and 1.51 g/cm^3, respectively. These values are in good agreement with values from theoretical, therefore suggesting very minimal porosities which likely from trapped gas during the fabrication process. Meanwhile, the difference between the experimental and theoretical density is most significant for UPR/30SA composite. The large difference between the densities values can be explained by the fact that the porous structure of SA particles has been impregnated by the resin, hence increase the density. However, it is noticed that the density of UPR/30SA is still much lower than the neat UPR, indicating that some parts of the SA pores were preserved from resin. In the case of composite with SA/ATH hybrid filler, the composite is 19% lighter (1.22 g/cm^3) than the UPR/30ATH (1.51 g/cm^3) by replacing 15 vol% of ATH with SA. Furthermore, the calculated porosity for the UPR/15ATH15SA was also higher than the UPR/30SA, suggesting a higher proportion of pores in the structure. Therefore, it is assumed that the contribution

to the porosity of the UPR/15ATH15SA by factors other than the SA pores itself should be considered. Among the possible factors could be the distribution and wettability of the hybrid filler in UPR.

Table 3: Experimental (Eρ) and theoretical (Tρ) density and relative porosity (Rϕ) of UPR and UPR composites

Composite	Eρ (g/cm^3)	Tρ (g/cm^3)	Rϕ (%)
UPR	1.14 ± 0.006	1.15	0.9 ± 0.05
UPR/30ATH	1.51 ± 0.013	1.53	1.3 ± 0.05
UPR/15ATH15SA	1.22 ± 0.016	1.32	7.5 ± 0.05
UPR/30SA	1.09 ± 0.022	0.83	5.2 ± 0.05

3.2 Tensile properties

The results of tensile tests are reported in Fig. 4, depicting the load versus extension curves for neat UPR and UPR composites. From the tensile curves, the mechanical properties such as tensile strength, strain and elastic modulus were derived as listed in Table 4. As observed in previous works on UPR composites containing silica [26] or alumina [27], the tensile properties increase with an increase in filler content within a low loading range (1 wt% - 40 wt%). In this study, indeed, the addition of SA, ATH and their combination has enhanced the tensile strength as well as elastic modulus but also results in ductility reduction through a restriction in the mobility of the UPR chain. The higher tensile strength and modulus observed for the composites containing single filler (UPR/30SA and UPR/30ATH), suggests better filler - matrix interfacial bonding. With respect to the neat UPR, the percentage increase in tensile strength of UPR/30ATH, UPR/30SA and UPR/15ATH15SA is 87%, 61% and 19%, respectively. The relatively smaller increase in tensile strength with the addition of SA/ATH hybrid is associated with the higher porosity of the resulting composite, acting as stress concentration sites that increase polymer segmental mobility [28].

For further analysis, the fracture surfaces of the broken tensile of UPR and UPR composites were examined under SEM–EDX. Fig. 5 shows the morphology of the fractured surface of neat UPR at 1000× magnification which failed at a tensile strength of 8.3 MPa. The brittle nature of UPR is clear from the SEM image, revealing a smooth fracture surface with micro-flow lines. Meanwhile, in Fig. 6 (a) and (c), the fracture surfaces of UPR/30ATH and UPR/30SA which failed at a maximum tensile strength of 15.5 and 13.3 MPa, respectively, exhibit more coarse and angular aggregates, revealing the interlocking mechanism, which results in high mechanical stiffness and elastic modulus [29]. In the case of the UPR/15ATH115SA, the morphology of fractured specimen at 9.8 MPa in Fig. 6 (b) exhibits more lumpy aggregates, due to the distribution of SA/ATH agglomerates of random sizes as revealed by the EDX mapping. As observed in previous studies [30], a drop in tensile strength is commonly related to agglomeration due to strong filler-filler interaction. In the present case, the ATH-SA agglomerates as seen in Fig. 6 (b) are only wetted on the outside, forming a barrier layer that

prevents internal wetting and results in undispersed lumps. These non-wetted or partially wetted volumes create porosity in the composite structure which consequently increases the polymer segmental mobility where crack can initiate and propagate, decreasing the tensile strength.

The dispersion of SA and ATH with a different dimension of agglomerates was also observed for composites with single filler as revealed by EDX elemental mapping in Fig. 6 (a1) and (c1), respectively. It is noticed that a more homogenous distribution of SA (Si element) can be observed in UPR/30SA whereas the ATH (Al element) tends to agglomerate. As demonstrated elsewhere [31-32] filler surface modification by grafting silane coupling agent is effective to achieve monodispersity by reducing the filler-filler interaction in the polymer while improving polymer-filler interaction. Herein, the influence of surface functionality on dispersibility could be observed on UPR/30SA. Better dispersibility of SA in UPR as compared to ATH is due to the coexistence of –OH and –CH3 groups on the SA surface which can form more linkages with UPR polar and non-polar groups.

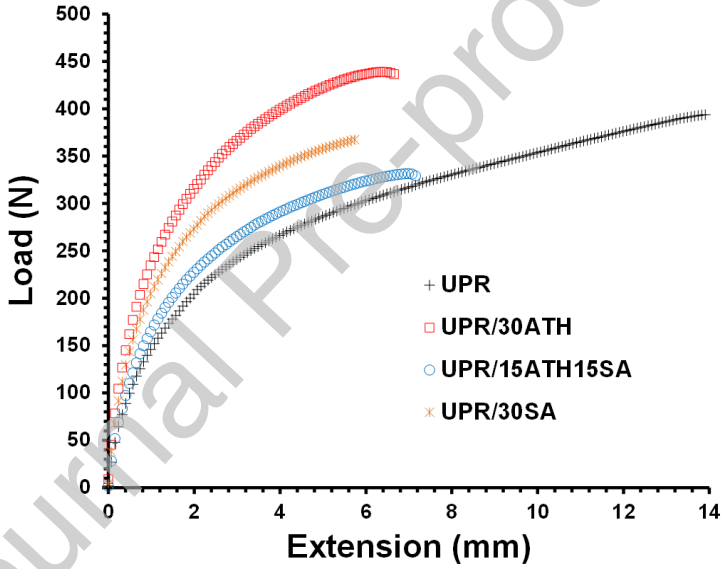

Fig. 4 Load versus extension curves of tensile test for UPR and UPR composites

Table 4: Mechanical properties of UPR and UPR composites

Sample	Tensile strength (MPa)	Tensile strain (%)	Elastic modulus (MPa)
UPR	8.28 ± 1.06	19.87 ± 2.10	49 ± 5.0
UPR/30SA	13.31 ± 3.73	9.27 ± 0.72	143 ± 13.8
UPR/30ATH	15.54 ± 4.06	8.08 ± 0.31	192 ± 24.3
UPR/15ATH15SA	9.84 ± 1.57	9.98 ± 0.42	90 ± 8.5

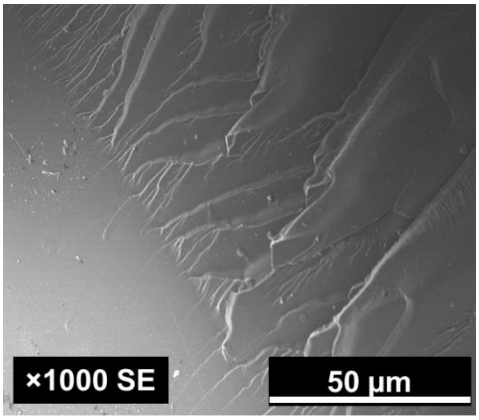

Fig. 5 SEM micrograph of the fracture surface of neat UPR

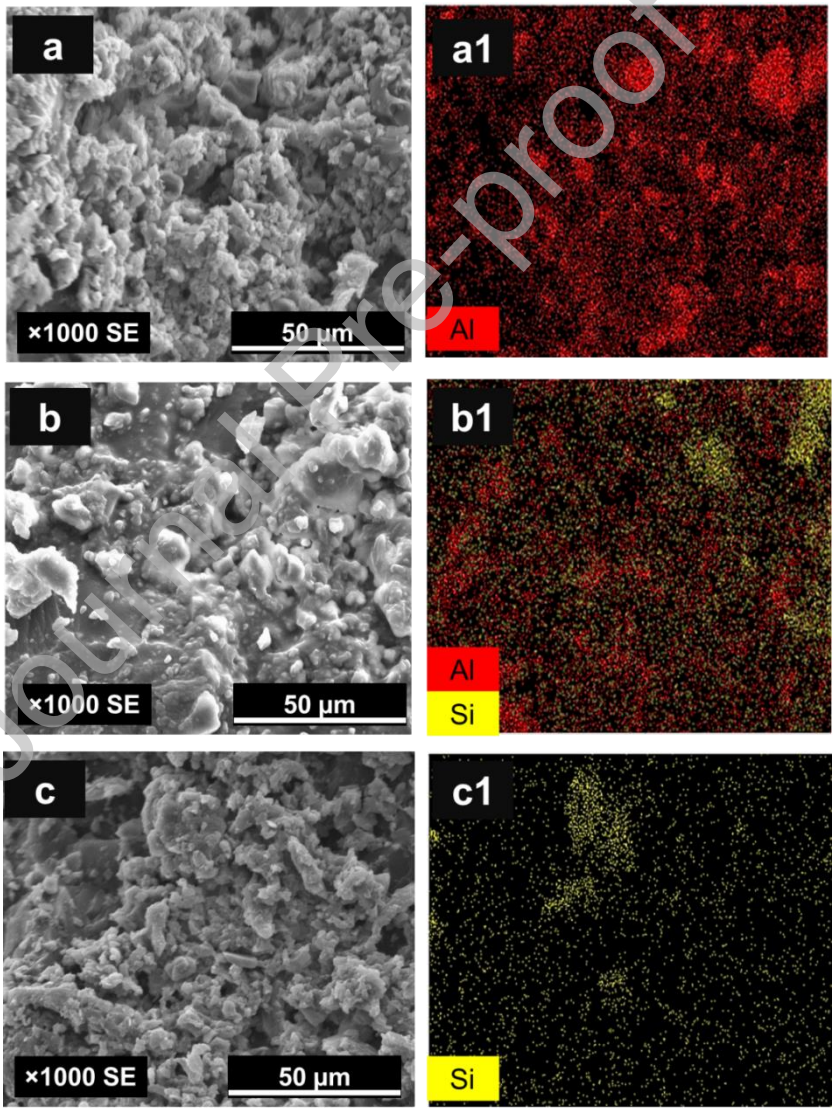

Fig. 6 SEM micrographs of tensile fracture surfaces of (a) UPR/30ATH (b) UPR/15ATH15SA (c) UPR/30SA and corresponding EDX elements mapping images (Al and Si refer aluminum and silicon).

3.3 Horizontal Burning (HB) Test

Table 5 shows the UL-94 horizontal burning test results of the neat UPR and UPR composites prepared in this study. It was observed that neat UPR and UPR/30SA samples burnt steadily with a ~0.28 mm/s and ~0.33 mm/s of burning rate upon ignition. Fire propagated until the entire samples were burnt, releasing thick smoke and airborne particles. The slight increase in the burning rate of the UPR/30SA however, did not indicate that the addition of SA has increased the flammability of the UPR, but due to the fuel replacement effect which speeds up the fire propagation. Conversely, the incorporation of ATH delivers the flame retardant characteristic to UPR as shown in the real-time images of the samples during the burning test in Fig. 7. Burning of the UPR/30ATH and UPR/15ATH15SA was ceased upon removal of the fire source after 6 and 13 s, respectively and the burning rate was not calculated as the fire did not pass the 25 mm reference mark. Hence, all of the investigated samples passed the HB (horizontal burning) class according to the ASTM D635-14 evaluation. Due to continuous burning, the neat UPR and UPR/30SA were classified as Class D, while UPR/30ATH and UPR/15ATH15SA have achieved Class B (flame retarded) as the fire was rapidly diminished after ignition [33].

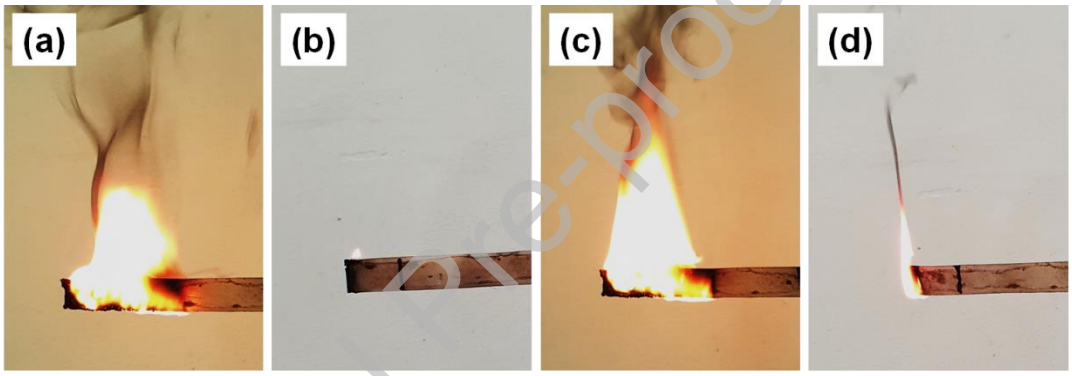

Fig. 7 Fire behavior of (a) Neat UPR (b) UPR/30ATH (c) UPR/30SA (d) UPR/15ATH15SA during the horizontal burning test

Table 5: UL 94 horizontal burning (ASTM D635-14) for UPR and UPR composites

Sample	Burning time (s)	Burn length (mm)	Burning rate (mm/s)	Rating class*[33]	Description
UPR	161	100	0.28	D	Thick, black smoke and airborne particles
UPR/30SA	153	100	0.33	D	Thick, black smoke and airborne particles
UPR/30ATH	6	< 25 mm	Self-extinguished	B	No smoke
UPR/15ATH15SA	13	< 25 mm	Self-extinguished	B	Minimal smoke, rapidly diminishing flame

A - There are no visible signs of combustion after the ignition source is removed
B - The flame front does not pass the 25 mm reference mark
C - The flame front passes the 25 mm reference mark but does not reach the 100 mm reference mark
D - The flame front reaches the 100 mm reference mark and the linear burning rate does not exceed 40 mm/min for specimens having a thickness between 3 and 13 mm or 75 mm/min for specimens having a thickness of less than 3 mm.

3.3 TGA of neat UPR and UPR composites

The thermal stability and decomposition behaviors of neat UPR and UPR composites were investigated by TGA under the air atmosphere to simulate a real working environment. Fig. 8 illustrates the weight percentage versus temperature (TGA curves) and the corresponding derivative thermogravimetry (DTG) curves for all samples. The maximum DTG peak simply refers to the point or temperature where the weight loss rate is maximum. Important information from TGA and DTG were summarized in Table 6. In general, the thermal decomposition of UPR can be explained based on three major steps. Initial decomposition was observed before 200 °C, involving less than 5wt% of weight loss, owing to the evaporation of moisture and uncured substances from the composite surfaces [5, 10]. Subsequently, the second step exhibits a steep weight loss between 250 °C to 400 °C with a maximum DTG peak of around 325 °C. This can be attributed to the major decomposition of UPR polymer via the rapid volatilization process [5, 10]. The final decomposition step is marked by the point at which the TGA and DTG curves start to return to their original baseline. Gradual weight loss as observed above 400°C is ascribed to the slow oxidation of thermal stable char yielded during the decomposition. For neat UPR, the TGA specimen is almost completely decomposed, leaving only a small amount of residue (1.8 wt%), mostly soot particles.

The addition of SA into UPR shows a negligible effect on the initial decomposition temperature ($T_{d\ onset}$) as the UPR/30SA and neat UPR decomposed at a similar temperature. However, the presence of SA could enhance the thermal stability at the higher temperature region as the maximum DTG peak for UPR/30SA was shifted to a higher temperature (340 ºC) with lower magnitude, indicating that the composite decomposed slowly than neat UPR, hence signaling for the possible barrier effect during the combustion process. Meanwhile, the decomposition of UPR/30ATH revealed an additional step process as marked by a distinct DTG peak between 220 °C and 280 °C, corresponding to mass loss of ATH by dehydration. Consequently, the released water vapor from the dehydration process has substantially reduced the decomposition rate of the UPR in which the sample shows the lowest magnitude of the DTG peak near 340 °C. Furthermore, the residue for UPR/30ATH was also the highest, around 30.5 wt%, mostly comprised of alumina (Al_2O_3). Compared to all samples, the incorporation of SA/ATH hybrid filler has shown an obvious improvement in the thermal stability of the UPR. This is evidenced by a remarkable shift of the maximum DTG peak toward higher temperatures for the UPR/15ATH15SA. Interestingly, there is no observable DTG peak representing the dehydration of ATH for UPR/15ATH15SA which previously observed for UPR/30ATH between 220 °C and 280 °C. In this case, a synergistic effect between ATH and SA during the thermal decomposition of UPR is suggested.

Table 6: TGA and DTG data under air atmosphere for neat UPR and UPR composites

Sample	$\mathbf{T_{d\ at\ 95wt\%}}$	$\mathbf{T_{d\ onset}}$	$\mathbf{T_{d\ max}}$	$\mathbf{T_{dfinal}}$	$\mathbf{R_{wt\%\ at\ 600°C}}$
UPR	188	275	325	400	1.8
UPR/30ATH	204	255	340	405	30.5
UPR/30SA	190	278	340	415	6.8
UPR/15ATH15SA	215	305	355	430	18.1

T_d, decomposition temperature; **$T_{d\ onset}$**, the intersection of a tangent to the inflection point and 100 wt% baseline; **T_{dmax}**, the temperature which highest change in weight loss occurred; **T_{dfinal}**, the point at which the DTG curve returns to its baseline; **$R_{wt\%}$**, the char residues at 600°C.

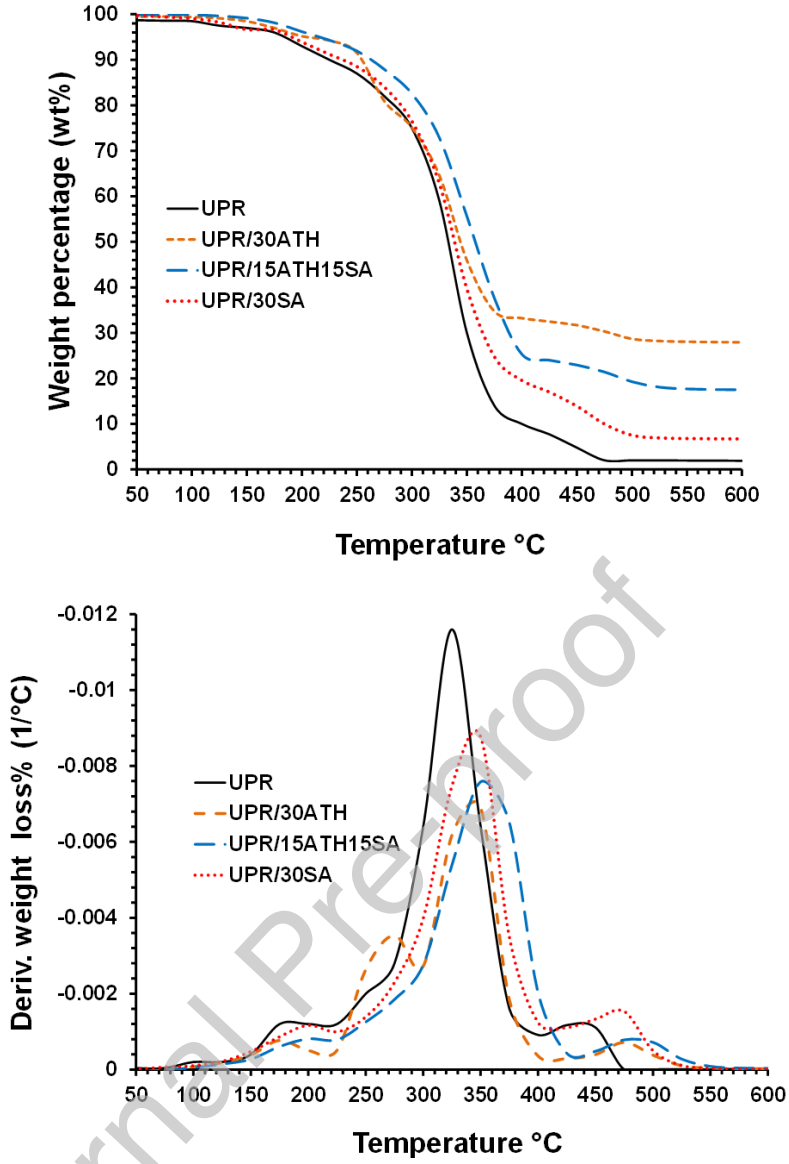

Fig. 8 TGA and DTG curves of UPR and UPR composites

3.4 TGA of ATH, SA and SA/ATH hybrid

Further, the synergism between ATH and SA was assessed by comparing the TGA-FTIR analysis of ATH, SA and the SA/ATH hybrid. The FTIR spectra were obtained near 325 ºC, to find out the contribution of the filler during the maximum mass loss rate of UPR. As already evidenced in previous work [4] and good agreement with our finding, the rapid mass loss of ATH via dehydration was occurred between 220-300ºC, with DTG peak near 270 ºC. As the FTIR spectrum collected at 325 ºC revealed no identifiable peak for ATH, it can be assumed that the dehydration process has been completed earlier. As already observed [34], the decomposition of SA is marked by a sharp DTG peak near 340 ºC, which is attributed to the oxidation of $–CH_3$ groups from the SA surface, releasing CO_2, CO and –OH gases as detected in the FTIR spectrum. Interestingly, when the ATH was

doped with SA as hybrid filler, the thermal stability and decomposition behavior of ATH changed obviously. The most significant change is described by the broader DTG peak between 220 – 350 ºC, where the gradual mass loss rate most likely implies prolonged dehydration for a wider temperature range. Therefore, a synergistic activity can be anticipated between SA and ATH, in which there is a combined effect of water release from ATH and also the production of CO_2 and CO from the oxidation of SA surface groups, as marked by strong FTIR peaks for SA/ATH hybrid. The inert gases (CO, CO_2, H_2O) generated during the decomposition of the hybrid filler can dilute the concentration of the volatiles and promote high char yield for UPR [35]. To get further insight regarding the synergism, the schematic of Fig. 10 illustrates the two important roles of SA in the condensed phase. First, it is proposed that the slower decomposition rate of ATH is due to the confinement effect by 3-dimensional nano-sized pores of SA which effectively inhibit the heat and mass transfer. Secondly, the oxidation of –CH3 groups from the SA surface also influences the formation of the carbonaceous layer which further enhances the thermal barrier effect. In summary, this finding should be able to explain why the composite with hybrid filler has demonstrated the highest thermal stability as compared to other composites with single filler.

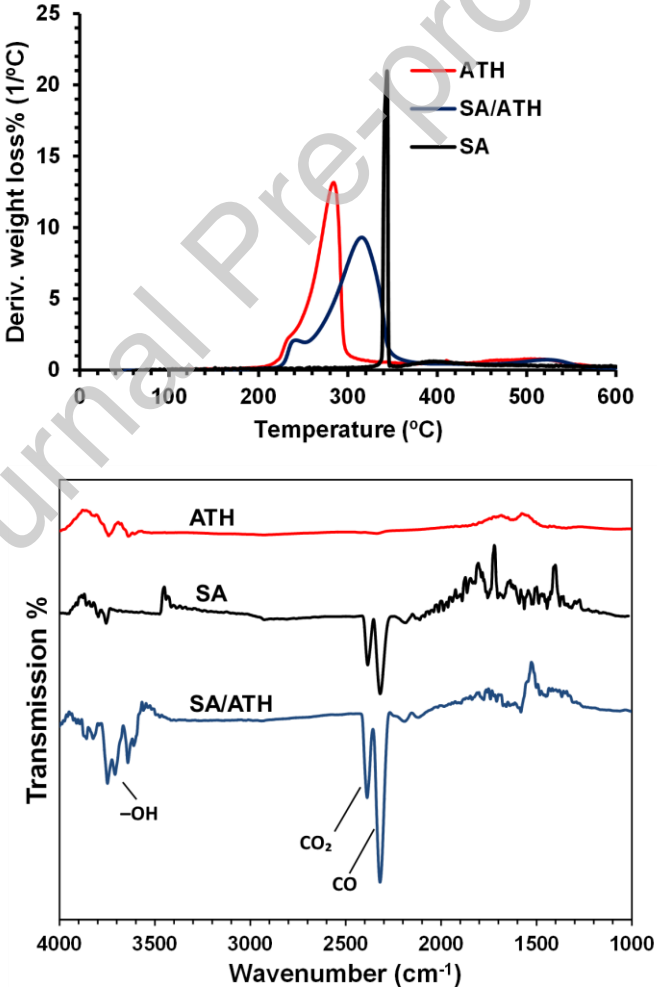

Fig. 9 Thermal decomposition and evolved gases analyses (DTG-FTIR) of filler materials under air atmosphere

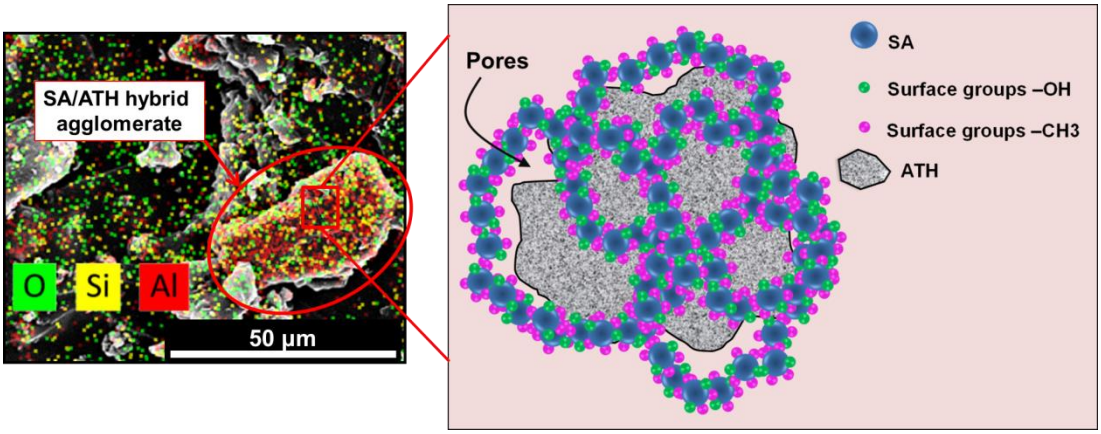

Fig. 10 SEM-EDX image of SA/ATH agglomerate in UPR matrix and schematic drawing illustrating the physical confinement of ATH within SA pore structure

3.5 DSC analysis of neat UPR and UPR composites

DSC analysis was employed to further determine the type and the approximate range of the thermal reaction during heating and also could be the indicator of the degree of thermal decomposition. Fig. 10 shows the plot of the reaction rate versus temperature of neat UPR and UPR composites in the temperature ranges of 200 ºC – 400 ºC, corresponding to the principal decomposition stage of UPR. The DSC curves of the four specimens can be divided into two stages and the information obtained from the thermal scans is summarized in Table 7. Stage 1 (200 °C – 300 °C) and Stage 2 (300 °C – 400 °C) represent the initial and the major UPR decomposition, respectively. Within Stage 1, no obvious thermal peak can be observed for neat UPR and UPR/30SA due to the slow reaction process, mostly involving the volatilization of styrene molecules [34]. For UPR/30ATH and UPR/15ATH15SA, each specimen revealed a broad endothermic curve between 230 °C – 300 °C, signaling the dehydration process of ATH. However, a peculiar sharp endothermic peak which superimposed on the broad endothermic curve of UPR/15ATH15SA can be observed near 250 °C. As observed in previous works [35], this peak is related to the phase transition of ATH ($Al_2O_3.3H_2O$) into $Al_2O_3.H_2O$ (Boehmite). In this case, the ATH – Boehmite transition for the hybrid filler could be favored by the presence of SA, which possibly rendered the dehydration process unstable. It is well known that the formation of Boehmite is favored by high partial pressures of water [35-36]. In this case, the SA may have impeded water escape during combustion, leading to high partial pressure and favor Boehmite formation. Partial dehydration of ATH via Boehmite transition yields a more gradual release of water over a wider temperature range as can be described by equations below [36];

$$Al_2O_3.3H_2O\ (ATH) \rightarrow Al_2O_3.H_2O\ (Boehmite) + 2\ H_2O \quad (1)$$

$$Al_2O_3.\ H_2O\ (Boehmite) \rightarrow Al_2O_3\ (Alumina) + H_2O \quad (2)$$

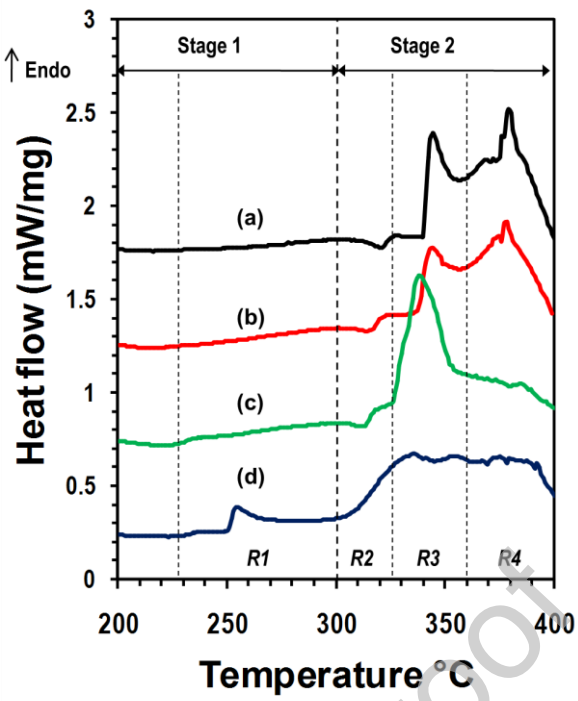

Fig. 11 DSC curves of (a) Neat UPR (b) UPR/30SA (c) UPR/30ATH and (d) UPR/15ATH15SA in the air atmosphere

Major decomposition of UPR within Stage 2 between 300 °C – 400 °C proceeds in three sub-stages (R2, R3, R4). Initially, a small exothermic peak can be seen near 300 °C – 320 °C for neat UPR, UPR/30SA and UPR/30ATH which referred to the ignition temperature of UPR [37-38]. However, the same peak was not observed for UPR/15ATH15SA, indicating that the addition of hybrid filler could seemingly eliminate the potential ignition of UPR. Above the ignition temperature, the specific heat starts to increase which in turn, results in the intense endothermic peaks as observe for all specimens within two sub-stages (R3, R4). For neat UPR, the oxidation process was represented by sharp double endothermic peaks as observed near 345 °C and 380 °C, respectively, associated with partial thermal decomposition [37-38]. This trend is followed by UPR/30SA, indicating that the addition of SA did not alter the decomposition behavior of UPR. The first endothermic peak is associated with the decomposition of ester linkages from the UPR backbone, whereas the second endothermic peak marks the decomposition of polystyrene network and aromatic hydrocarbons [38]. Nevertheless, the intensity of these peaks for UPR/30SA is slightly lower than the neat UPR, signaling a slower transformation process. Contrary, the major decomposition process of UPR/30ATH is represented by a single sharp endothermic peak at approximately 335 °C, indicating a rapid transformation process. It can be deduced that the release of ATH water during Stage 1, is responsible for diluting the volatiles (gas phase), maintaining the thermal stability of UPR. However, as the temperature increased and the water has completely evaporated, the remaining portion of the specimen begins to decompose rapidly, leading to an intense endothermic reaction. In a comparison of the major decomposition process of UPR/15ATH15SA with other specimens, the composite exhibits a shallow and broad endothermic region between 330 °C – 390 °C. This slow and steady decomposition

process confirms the role of SA/ATH hybrid in improving the thermal stability of UPR, which previously in agreement with the TGA-DTG result.

Table 7: Results of DSC analyses for UPR and UPR composites

	Thermal events			
	R1 (Endothermic) Dehydration (ATH)	*R2 (Exothermic) Ignition point*	*R3 (Endothermic) 1st Decomposition*	*R4 (Endothermic) 2nd Decomposition*
Sample	**Peak temperature °C**			
UPR	-	320	345	380
UPR/30SA	-	317	345	380
UPR/30ATH	230 – 300	312	335	-
UPR/15ATH15SA	250	-	330 – 390	-

4.0 FTIR spectra of evolved gas products

A further comparison of the volatile species evolved by thermal decomposition of the UPR samples is shown by the FTIR spectra of Fig. 12 as obtained near the maximum decomposition rate (300 – 350 ºC). Table 8 lists the gaseous products corresponding to the transmittance peaks. As for neat UPR, the gaseous decomposition products are hydrocarbons, carbonyl compounds, anhydrides, and aromatic species. With the addition of fillers, the peaks of CO and CO_2 appeared around 2300 cm^{-1} and also H_2O (3500 – 3800 cm^{-1}). A more intense CO peak as observed near 2305 cm^{-1} is the result of incomplete oxidation of char during the combustion process [40]. It is noticeable that the FTIR peak intensities for UPR/30SA and UPR/15ATH15SA specimens were lower than the neat UPR and UPR/30ATH, indicating a lower amount of released gases. The amount also appears to be in good accordance with the degree of the reaction during the R3 temperature region as marked by endothermic peaks in the DSC analysis. For example, the UPR/30ATH shows the most intense endothermic peak within the R3 temperature region which is associated with rapid volatilization; therefore the process is marked by strong FTIR peaks of the gas phase. Besides, it is revealed that the addition of SA could reduce the amount of gases released during the decomposition of UPR, as the nano-porous structure of the SA is effective in inhibiting mass and heat transport.

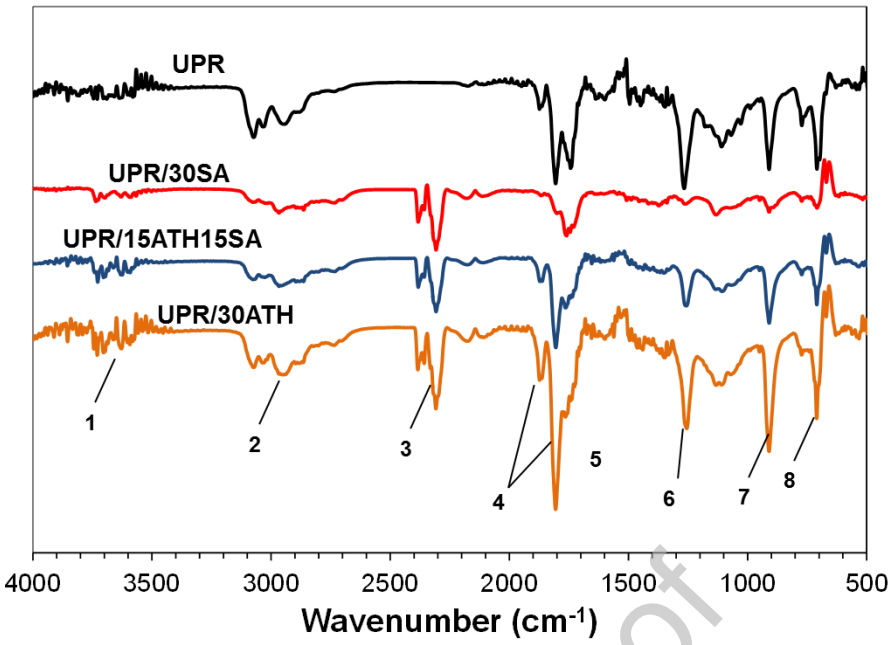

Fig. 12 FTIR spectra of the gas species produced during TGA of the UPR and UPR composites at maximum decomposition temperature.

Table 8: FTIR peaks assignment of the volatile species during thermal decomposition of the UPR [40]

Peak No.	Wavenumber (cm^{-1})	Volatile species
1	3500–3800	–OH (H_2O, phenols)
2	3150–2900	C–H (hydrocarbons)
3	2390–2305	CO2, CO
4	1870–1805	CH3COCH3, CH3COOH (anhydrides)
5	1760–1740	C=O (carbonyls)
6	1250–1140	C–O–C (esters)
7	910	C-H, C-O (anhydrides)
8	710	C–H (aromatic rings)

4.0 Conclusions

In this study, a hybrid of SA/ATH was proposed as a new FR additive in UPR to overcome the shortcomings of conventional ATH relating to its thermal stability and weight. Four samples, consisting of a neat UPR and three UPR composites comprising ATH, SA, and SA/ATH hybrid were prepared, respectively. The performance of SA/ATH hybrid was evaluated through a comparative analysis of physio-mechanical and thermal decomposition behavior of the samples as obtained from several tests; covering density and porosity measurement, SEM-EDX, tensile properties, horizontal burning test, TGA-FTIR and DSC. From the physio-mechanical perspectives, the UPR/15ATH15SA with a density of 1.22 g/cm^3, was at least 19% lighter than the composite containing only ATH (UPR30ATH). However, the addition of SA/ATH hybrid only contributes to an approximately 18% increase in the tensile strength of UPR while the addition of only ATH or SA has increased the tensile strength by 87% and 60 %, respectively. The lower degree of mechanical reinforcing capability of SA/ATH hybrid is because of a strong filler-filler attraction between SA and ATH which leads to porosity and agglomeration as evidenced by density measurements and SEM micrography. Nevertheless, we believed that the mechanical properties of the UPR can be further improved by refining the particle sizes of the SA/ATH hybrid. From the physical observation on the fire propagation during the horizontal burning test, it is safe to conclude that the addition of SA/ATH hybrid into UPR could provide sufficient flame retardancy by imparting self-extinguishing characteristics to UPR. From a thermal performance point of view, the combination of ATH and SA exhibits an evident synergistic effect in which the heat and mass barrier effect of SA could prolong the endothermic decomposition of ATH, resulting in a more gradual release of water over a wider range of temperatures. The TGA/DTG analysis show that the decomposition temperature (DTG peak) of UPR15ATH15SA, was at least 30 ºC and 15 ºC higher than that of the decomposition temperature of neat UPR and UPR composites with single filler, respectively. The evolved gas products were analyzed by FTIR at the maximum decomposition rate of UPR, indicating that the addition of SA and the SA/ATH hybrid can decline the release of volatile gas, resulting into a more thermally stable condensed phase at higher temperature as confirmed by DSC behavior of the UPR samples during major decomposition process (300 ºC – 400 ºC).

Author's Declaration

On behalf of all Co-Authors, the corresponding author states that there is no conflict of interest. The corresponding author shall bear full responsibility for the submission and this research has not been submitted for publication elsewhere. We attest to the fact that all authors listed on the title page have contributed significantly to the work, have read the manuscript, attest to the validity and legitimacy of the data and its interpretation, and agree to its submission to this journal.

References

[1] Flame retardants - higher performance and wider product choice. (2003). Plastics, Additives and Compounding, 5(6), 32–36. https://doi.org/10.1016/S1464-391X(03)00042-4

[2] Reuter, J., Greiner, L., Kukla, P., & Döring, M. (2020). Efficient flame retardant interplay of unsaturated polyester resin formulations based on ammonium polyphosphate. Polymer Degradation and Stability, 178, 109134. https://doi.org/10.1016/j.polymdegradstab.2020.109134

[3] Tibiletti, L., Longuet, C., Ferry, L., Coutelen, P., Mas, A., Robin, J.-J., & Lopez-Cuesta, J.-M. (2011). Thermal degradation and fire behaviour of unsaturated polyesters filled with metallic oxides. Polymer Degradation and Stability, 96(1), 67–75. https://doi.org/10.1016/j.polymdegradstab.2010.10.015

[4] Wang, Y., Zhang, L., Yang, Y., & Cai, X. (2016). Synergistic flame retardant effects and mechanisms of aluminum diethylphosphinate (AlPi) in combination with aluminum trihydrate (ATH) in UPR. Journal of Thermal Analysis and Calorimetry, 125(2), 839–848. https://doi.org/10.1007/s10973-016-5459-x

[5] Salasinska, K., Celiński, M., Barczewski, M., Leszczyński, M. K., Borucka, M., & Kozikowski, P. (2020). Fire behavior of flame retarded unsaturated polyester resin with high nitrogen content additives. Polymer Testing, 84, 106379. https://doi.org/10.1016/j.polymertesting.2020.106379

[6] Shaw, S. D., Blum, A., Weber, R., Kannan, K., Rich, D., Lucas, D., … Birnbaum, L. S. (2010). Halogenated flame retardants: do the fire safety benefits justify the risks? Reviews on Environmental Health, 25(4), 261–305. https://doi.org/10.1515/reveh.2010.25.4.261

[7] Troitzsc, J. H. (2013). Fires, Fire Safety and Trends. Regulations, Standards and the Role of Flame Retardancy. International Polymer Science and Technology, 40(10), 1–6. https://doi.org/10.1177/0307174X1304001001

[8] Hull, T. R., Witkowski, A., & Hollingbery, L. (2011). Fire retardant action of mineral fillers. Polymer Degradation and Stability, 96(8), 1462–1469. https://doi.org/10.1016/j.polymdegradstab.2011.05.006

[9] Levinţa, N., Vuluga, Z., Teodorescu, M., & Corobea, M. C. (2019). Halogen-free flame retardants for application in thermoplastics based on condensation polymers. SN Applied Sciences, 1(5), 422. https://doi.org/10.1007/s42452-019-0431-6

[10] Kandola, B. K., & Ebdon, J. R. (2019). Chapter 17 - Flammability and Thermal Stability of Unsaturated Polyester Resin-Based Blends and Composites. In S. Thomas, M. Hosur, & C. J. Chirayil (Eds.), Unsaturated Polyester Resins (pp. 435–469). Elsevier. https://doi.org/10.1016/B978-0-12-816129-6.00017-X

[11] Kandare, E., Kandola, B. K., Price, D., Nazaré, S., & Horrocks, R. A. (2008). Study of the thermal decomposition of flame-retarded unsaturated polyester resins by thermogravimetric analysis and Py-GC/MS. Polymer Degradation and Stability, 93(11), 1996–2006. https://doi.org/10.1016/j.polymdegradstab.2008.03.032

[12] Suoware, T. O., Edelugo, S. O., & Ezema, I. C. (2019). Impact of hybrid flame retardant on the flammability and thermomechanical properties of wood sawdust polymer composite panel. Fire and Materials, 43(4), 335–343. https://doi.org/10.1002/fam.2704

[13] Lou, F., Wu, K., Wang, Q., Qian, Z., Li, S., & Guo, W. (2019). Improved Flame-Retardant and Ceramifiable Properties of EVA Composites by Combination of Ammonium Polyphosphate and Aluminum Hydroxide. Polymers, 11(1). https://doi.org/10.3390/polym11010125

[14] Riahipour, R., Sahraei, A. A., Werken, N. van de, Tehrani, M., Abrinia, K., & Baniassadi, M. (2018). Improving flame-retardant, thermal, and mechanical properties of an epoxy using halogen-free fillers. Science and Engineering of Composite Materials, 25(5), 939–946. https://doi.org/10.1515/secm-2017-0131

[15] Chen, Z., Jiang, M., Zhang, Q., Yu, Y., Sun, G., & Jiang, J. (2017). Synergistic effect of combined dimethyl methylphosphonate with aluminum hydroxide or ammonium polyphosphate retardant systems on the flame retardancy and thermal properties of unsaturated polyester resin. International Journal of Polymer Analysis and Characterization, 22(6), 509–518. https://doi.org/10.1080/1023666X.2017.1331393

[16] Yang, X., Shen, A., Su, Y., & Zhao, W. (2020). Effects of alumina trihydrate (ATH) and organic montmorillonite (OMMT) on asphalt fume emission and flame retardancy properties of SBS-modified asphalt. Construction and Building Materials, 236, 117576. https://doi.org/10.1016/j.conbuildmat.2019.117576

[17] Chang, M.-K., Hwang, S.-S., & Liu, S.-P. (2014). Flame retardancy and thermal stability of ethylene-vinyl acetate copolymer nanocomposites with alumina trihydrate and montmorillonite. Journal of Industrial and Engineering Chemistry, 20(4), 1596–1601. https://doi.org/10.1016/j.jiec.2013.08.004

[18] Pan, Y., He, S., Cheng, X., Li, Z., Li, C., Huang, Y., & Gong, L. (2017). A fast synthesis of silica aerogel powders-based on water glass via ambient drying. Journal of Sol-Gel Science and Technology, 82(2), 594–601. https://doi.org/10.1007/s10971-017-4312-4

[19] Dourbash, A., Buratti, C., Belloni, E., & Motahari, S. (2017). Preparation and characterization of polyurethane/silica aerogel nanocomposite materials. Journal of Applied Polymer Science, 134(8). https://doi.org/10.1002/app.44521

[20] Kim, H. M., Kim, H. S., Kim, S. Y., & Youn, J. R. (2015). Silica aerogel/epoxy composites with preserved aerogel pores and low thermal conductivity. E-Polymers, 15(2), 111–117. https://doi.org/10.1515/epoly-2014-0165

[21] Halim, Z. A. A., Yajid, M. A. M., Idris, M. H., & Hamdan, H. (2018). Effects of Rice Husk Derived Amorphous Silica on the Thermal-Mechanical Properties of Unsaturated Polyester Composites. Journal of Macromolecular Science, Part B, 57(6), 479–496. https://doi.org/10.1080/00222348.2018.1476440

[22] Abdul Halim, Z. A., Mat Yajid, M. A., Idris, M. H., & Hamdan, H. (2018). Physiochemical and thermal properties of silica Aerogel–Poly vinyl alcohol / Core–Shell structure prepared using fluidized bed coating process for thermal insulation applications. Materials Chemistry and Physics, 215, 269–276. https://doi.org/10.1016/j.matchemphys.2018.05.019

[23] Halim, Z. A. A., Yajid, M. A. M., & Hamdan, H. (2020). Effects of Solvent Exchange Period and Heat Treatment on Physical and Chemical Properties of Rice Husk Derived Silica Aerogels. Silicon. https://doi.org/10.1007/s12633-020-00421-5

[24] Chirayil, C. J., Mathew, L., Hassan, P. A., Mozetic, M., & Thomas, S. (2014). Rheological behaviour of nanocellulose reinforced unsaturated polyester nanocomposites. International Journal of Biological Macromolecules, 69, 274–281. https://doi.org/10.1016/j.ijbiomac.2014.05.055

[25] Chirayil, C. J., Joy, J., Mathew, L., Koetz, J., & Thomas, S. (2014). Nanofibril reinforced unsaturated polyester nanocomposites: Morphology, mechanical and barrier properties, viscoelastic behavior and polymer chain confinement. Industrial Crops and Products, 56, 246–254. https://doi.org/10.1016/j.indcrop.2014.03.005

[26] Sequeira, D., Mascarenhas, J., Picardo, D., Dias, R., & Sutari, O. (2015). Mechanical Behaviour of Fumed Silica/Glass Reinforced Polyester Nanocomposites. American Journal of Materials Science, 5(3C), 92–95.

[27] Ahmad, T., Raza, S. S., Aleem, E., Kamran, M., Manzoor, U., Makhdoom, A., Ahmad, R., & Mukhtar, S. (2017). Improvement in mechanical and thermal properties of unsaturated polyester- based hybrid composites. Iranian Polymer Journal, 26(4), 305–311. https://doi.org/10.1007/s13726-017-0520-6

[28] Jose, J. P., & Thomas, S. (2014). XLPE based Al2O3–clay binary and ternary hybrid nanocomposites: self-assembly of nanoscale hybrid fillers, polymer chain confinement and transport characteristics. Physical Chemistry Chemical Physics, 16(37), 20190–20201. https://doi.org/10.1039/C4CP03403A

[29] Hong, L., Gu, X., & Lin, F. (2014). Influence of aggregate surface roughness on mechanical properties of interface and concrete. Construction and Building Materials, 65, 338–349. https://doi.org/10.1016/j.conbuildmat.2014.04.131

[30] Biswas, B., Bandyopadhyay, N. R., & Sinha, A. (2019). Chapter 16 - Mechanical and Dynamic Mechanical Properties of Unsaturated Polyester Resin-Based Composites. In S. Thomas, M. Hosur, & C. J. Chirayil (Eds.), Unsaturated Polyester Resins (pp. 407–434). Elsevier. https://doi.org/10.1016/B978-0-12-816129-6.00016-8

[31] Mishra, S., Misra, M., Tripathy, S. S., Nayak, S. K., & Mohanty, A. K. (2001). Potentiality of Pineapple Leaf Fibre as Reinforcement in PALF-Polyester Composite: Surface Modification and Mechanical Performance. Journal of Reinforced Plastics and Composites, 20(4), 321–334. https://doi.org/10.1177/073168401772678779

[32] Nandi, S., Bose, S., Mitra, S., & Ghosh, A. K. (2013). Dynamic rheology and morphology of HDPE-fumed silica composites: Effect of interface modification. Polymer Engineering & Science, 53(3), 644–650. https://doi.org/10.1002/pen.23299

[33] Crossley, R., Schubel, P., & Stevenson, A. (2013). Furan matrix and flax fibre as a sustainable renewable composite: Mechanical and fire-resistant properties in comparison to phenol, epoxy and polyester: Journal of Reinforced Plastics and Composites. https://doi.org/10.1177/0731684413502108

[34] Li, Z., Cheng, X., Shi, L., He, S., Gong, L., Li, C., & Zhang, H. (2016). Flammability and oxidation kinetics of hydrophobic silica aerogels. Journal of Hazardous Materials, 320(Supplement C), 350–358. https://doi.org/10.1016/j.jhazmat.2016.07.054

[35] Decleer, J. G. M. (2010). TG/XRD/Sem Study of the Conversion of Gibbsite to (Pseudo) Boehmite. Bulletin Des Sociétés Chimiques Belges, 98(7), 449–462. https://doi.org/10.1002/bscb.19890980704

[36] Zhu, Y., Otsubo, M., Honda, C., & Ohno, A. (2005). Suppression effect of ATH filler on the erosion of filled silicone rubber exposed to dry band arc discharge. Polymer Testing, 24(7), 893–899. https://doi.org/10.1016/j.polymertesting.2005.06.007

[37] Budrugeac, P. (2000). The evaluation of the non-isothermal kinetic parameters of the thermal and thermo-oxidative degradation of polymers and polymeric materials: its use and abuse. Polymer Degradation and Stability, 71(1), 185–187. https://doi.org/10.1016/S0141-3910(00)00148-8

[38] Kicko-Walczak, E. (2003). Kinetics of thermal decomposition of unsaturated polyester resins with reduced flammability. Journal of Applied Polymer Science, 88(13), 2851–2857. https://doi.org/10.1002/app.11723

[39] Salasinska, K., Celiński, M., Barczewski, M., Leszczyński, M. K., Borucka, M., & Kozikowski, P. (2020). Fire behavior of flame retarded unsaturated polyester resin with high nitrogen content additives. Polymer Testing, 84, 106379. https://doi.org/10.1016/j.polymertesting.2020.106379

[40] Lin, Y., Jiang, S., Hu, Y., Chen, G., Shi, X., & Peng, X. (2018). Hybrids of aluminum hypophosphite and ammonium polyphosphate: Highly effective flame retardant system for unsaturated polyester resin. Polymer Composites, 39(5), 1763–1770. https://doi.org/10.1002/pc.24128

CRediT author statement

Zulhelmi Alif Abdul Halim:

Conceptualization, Methodology, Visualization, Writing - Original Draft

Muhamad Azizi Mat Yajid:

Validation, Writing - Review & Editing, Funding acquisition

Fajar Anugrah Nurhadi:

Investigation

Norhayati Ahmad:

Supervision, Project administration

Halimaton Hamdan:

Resources, Supervision

Declaration of interest statement

On behalf of all Co-Authors, the corresponding author states that there is no conflict of interest. The corresponding author shall bear full responsibility for the submission and this research has not been submitted for publication elsewhere. We attest to the fact that all authors listed on the title page have contributed significantly to the work, have read the manuscript, attest to the validity and legitimacy of the data and its interpretation, and agree to its submission to this journal.